Journal of GeoEngineering, Vol. 10, No. 3, pp. 91-103, December 2015
http://dx.doi.org/10.6310/jog.2015.10(3).3

BICONCAVE BOND MODEL FOR CEMENTED GRANULAR MATERIAL

Chia-Chi Chiu[1*], Meng-Chia Weng[2], and Tsan-Hwei Huang[3]

ABSTRACT

This study presents a biconcave bond model for use with the distinct element method (DEM) to simulate cementation efficacy between two particles in granular materials. The proposed model adopts a more realistic shape of cementation and considers the elastic response of cementation under external loading. The stress field and force-displacement relationship of biconcave bond model are assessed according to the Dvorkin theory. To apply the theory to DEM analysis, a modified superposition method was used to improve the accuracy and symmetry of the stress field. To assess the validity of the modified Dvorkin theory, we compared the deformation behaviors with the numerical elastic analysis by using the finite element method (FEM). The stress field calculated using the modified Dvorkin theory was consistent with FEM result and was able to solve the reaction when two particles were in arbitrary motion. The proposed model was further verified with the behavior of assemblies of cemented aluminum rod. The results demonstrate that the model is effective with the cemented granular material under different compressive conditions. In addition, the required parameters of the proposed model can be acquired from the bond material properties rather than through conventional back calculation. This model provides an innovative means to simulate the behavior of cemented granular material.

Key words: Bond, cementation, distinct element method (DEM), granular material.

1. INTRODUCTION

In recent years, the distinct element method (DEM) has been widely adopted to simulate the behavior of granular materials such as sand (Chang *et al*. 2012; Wang *et al*. 2014), concrete (Kozicki and Donzé 2008), and rock (Potyondy and Cundall 2004; Mas Ivars *et al*. 2011; Weng and Li 2012; Chiu *et al*. 2013; Duan *et al*. 2015). Compared with continuum analysis, the DEM has several unique characteristics and advantages, such as the ability to simulate crack propagation and large deformation problems, which is suitable for analysis some geological hazards like earthquake-induced rockfall or landslide. The discrete characteristics of DEM make it superior to other geotechnical analysis methods in failure simulation, but these features also increase the complexity of the method. One major difficulty is determining the contact relationships between particles (Potyondy and Cundall 2004, Ng 2006).

The contact relationship between particles (*i.e.*, contact model) was discovered by Hertz (Hertz 1882). He developed the elastic contact theory, which considers interaction between two circular particles. Subsequently, numerous contact models were proposed to describe various characteristics such as viscosity and displacement softening (Walton and Braun 1986, ItascaConsultingGroup 2015). Other than the contact theories of cohesionless granular materials, Potyondy and Cundall (2004) proposed a parallel bond model based on Euler-Bernoulli beam theory to simulate the behavior of cemented particles, such as rock and concrete. This model is widely used in the practice of rock engineering. Furthermore, Jiang and Zhu (2007) designed a bond model that contains a limited bond area comprising a series of elastic-dashpot contacts; Delenne *et al*. (2004) developed failure criteria for bond layers on the basis of experimental results; Obermayr *et al*. (2013) derived a bond model based on the Timoshenko beam theory; Pilkavičius *et al*. (2013) calculated the ratio of occupied length between particles and bond layers in the Timoshenko beam theory to determine the corresponding bond stiffnesses; Brown (2014) used the 3D Timoshenko beam in a DEM simulation; Potyondy (2011) modified the calculations of moment part in a parallel bond model to correct the ratio of unconfined compressive strength to tensile strength value; and Ding and Zhang (2014) discussed this modification in more detail, changing both normal and shear parts of moment calculations. These bond models advanced the simulation of bond behavior considerably. However, most of the models are based on the linear spring model or the Timoshenko beam model and do not consider the real shape of the bond layer. To appear the reality of bond shape, Dvorkin *et al*. (1991) presented a simplified elastic theory of a biconcave bond layer, reducing the obtained stress field to an elastic foundation to calculate particle reaction, then using a similar formula to investigate particle-cement behavior under pre-compacted conditions (Dvorkin and Yin 1995). Zhu *et al*. (1996) considered the shape influence of a biconcave elastic binder and determined bond behavior by using a Boussinesq equation based on a half-space premise; however, the stress field of the bond layer was still simplified to a unified elastic foundation, rather than considering the real shape. Therefore, to determine the comprehensive mechanical behavior of the bond layer, we developed a bond model for DEM, which considers bond geometry and the reactions of the bond layer.

Manuscript received July 22, 2015; revised November 25, 2015; accepted November 26, 2015.
[1] Ph.D candidate, Department of Civil Engineering, National Taiwan University, Taipei 10617, Taiwan.
[2] Professor (corresponding author), Department of Civil and Environmental Engineering, National University of Kaohsiung, Kaohsiung University Rd., Taiwan(e-mail: mcweng@nuk.edu.tw).
[3] Professor, Department of Civil Engineering, National Taiwan University, Taipei 10617, Taiwan.

From the micro image of an cemented granular intact rock sample (Figs. 1(a) and 1(b)), the shapes of cementation between particles usually resemble biconcave shape (Fig. 1(c)), which represents the mechanical behavior of bond based on biconcave shape is more reasonable than rectangular shape in cemented granular material. Therefore, this study propose a bond model considering the deformation behavior of biconcave shape, and the proposed model in this study was named the biconcave bond model (Fig. 1(d)). The theory of biconcave bond model for DEM originated from the Dvorkin elastic theory. Comparing with the parallel bond model, the major difference between these two bond models is bond shape (Fig. 2): the parallel bond model uses a rectangular bond whereas the biconcave bond model considers the bond a biconcave layer, which is more similar to natural cementation.

This paper first introduces the basic theory of the biconcave model and uses two methods to improve the accuracy and applicability of the model in section 2 and 3. The construction of biconcave bond model is reported in section 4. The stress contours of the bond layer of the biconcave model are then presented and compared with a finite element method (FEM) elastic analysis in section 5. Finally, the application of biconcave bond model, implemented with DEM Particle Flow Code 2 dimension (PFC2D) software is reported in section 6.

2. ELASTIC RESPONSE OF BOND LAYERS

The basic theory of biconcave bond model is based on the Dvorkin theory (Dvorkin *et al*. 1991), which describes the elastic behavior of a specific geometry bond layer under external displacement. This study provides two improvements to increase the accuracy of stress fields and compatibility with numerical analysis. To apply the Dvorkin simplified elastic analysis to calculations, the following must be assumed regarding the biconcave bond:

1. The particles are treated as 2D circular rigid bodies with finite mass.
2. The particles are much stiffer than cement materials. Thus, the Dvorkin theory applies and the model tends to simulate particle-cemented material.
3. The biconcave bond exhibits elastic behavior.
4. The biconcave bond is virtual in numerical analysis and it does not affect the arrangement of particles.

Figure 3 shows the geometry of the bond layer, where $W(x)$ and $U(x)$ are displacements of the upper particle surface, which can be considered upper particle movement. The terms $u_z(x, z)$ and $u_x(x, z)$ are the displacement fields of the bond layer, $h(x)$ is the thickness, and t and w are the bond thickness and radii factor, respectively, which determine the thickness and radius of the bond layer, which is assumed to be related to the ratio of the smaller particle's radius. The term $t = 0.2$ indicates that the thickness of the bond layer is 20% of the smaller particle's radius.

In a particle's translation motion, $W(x)$ and $U(x)$ can be obtained easily by analyzing the particle's normal and shear motion, which are treated as constants W_{const} and U_{const}, respectively. For rotating particles, $W(x)$ and $U(x)$ are functions of the particle's rotational angle. Equations (1a) and (1b) describe the amount of total displacement along the particle surface:

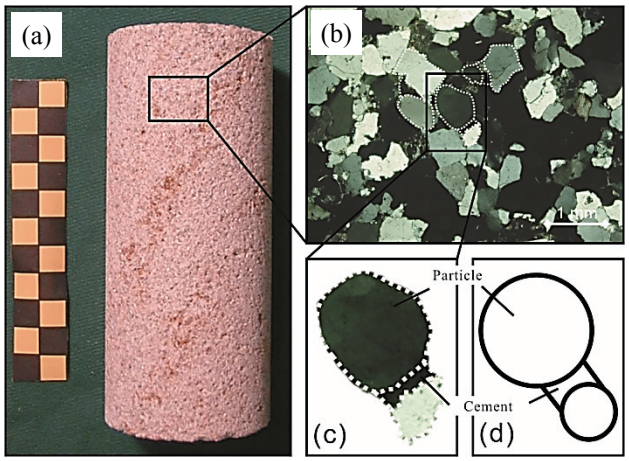

Fig. 1 Bond between particles in sedimentary rock and the concept of the proposed model. (a) Intact sandstone specimen; (b) Microscopic image of sandstone; (c) Grain and matrix; (d) Schematic particle and cement

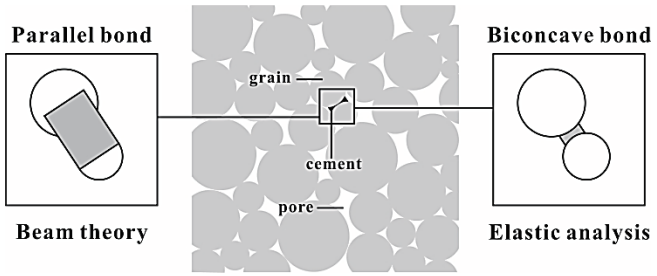

Fig. 2 Difference between parallel bond theory and biconcave bond theory

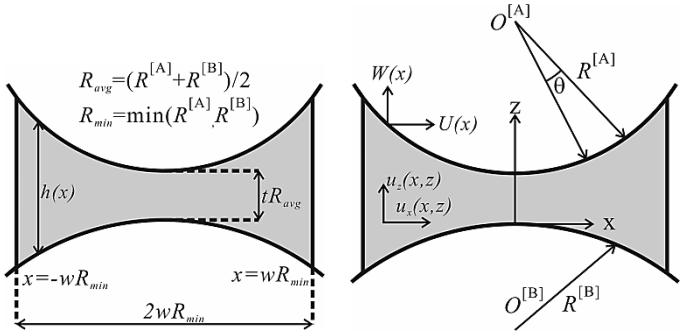

(a) Geometry (b) Coordinates of a bond layer

Fig. 3 Geometry and coordinates of a bond layer

$$U(x) = U_{const} + 2R_1 \sin\frac{\theta}{2}\sin\left(\frac{\theta}{2} + \cos^{-1}\left(-\frac{x}{R_1}\right)\right) \quad (1a)$$

$$W(x) = W_{const} - 2R_1 \sin\frac{\theta}{2}\cos\left(\frac{\theta}{2} + \cos^{-1}\left(-\frac{x}{R_1}\right)\right) \quad (1b)$$

where θ is the rotational angle, R_1 is the radius of the upper particle, and the origin of x is located at the center of the particle.

To obtain a simplified elastic theory, first the displacement field in bond are assumed as:

$$u_x(x, z) = \alpha(x)z + \beta(x)z^2 \quad (2a)$$

$$u_z(x, z) = \varepsilon(x)z \quad (2b)$$

The $\alpha(x)$, $\beta(x)$ and $\varepsilon(x)$ are the parameters to be evaluated. If the coordinate system is assumed connected with the surface of bottom grain, the below equation can be obtained:

$$\varepsilon(x) = W(x) / h(x) \tag{3a}$$

$$\alpha(x) = U(x) / h(x) - \beta(x) h(x) \tag{3b}$$

From the Hook's law for the plane theory of elasticity and the equations of static elasticity, Eqs. (4a) and (4b) can be derived, and $\beta(x)$ can be solved (Dvorkin *et al*. 1991):

$$\beta''(x) + A(x)\beta'(x) + B(x)\beta(x) = C(x) \tag{4a}$$

$$A(x) = 6h'(x) / h(x), \quad B(x) = \frac{3}{h(x)}\left[h''(x) - \frac{2(1-2v)}{h(x)(1-v)} \right].$$

$$C(x) = \frac{3}{h(x)}\left[\delta''(x) + \frac{\varepsilon'(x)}{h(x)(1-v)} \right]$$

$$\delta(x) = U(x) / h(x), \text{ and } \varepsilon(x) = W(x) / h(x)$$

where v is the Poisson's ratio of cement. The boundary conditions can be expressed as

$$\beta'(x) + \beta(x)\frac{3h'(x)}{h(x)} = \frac{6}{h(x)}\left[\frac{\delta'(x)}{2} + \frac{\varepsilon(x)v}{h(x)(1-v)} \right] \tag{4b}$$

After $\beta(x)$ is obtained, the stress and displacement field of the bond layer can be calculated, and the current forces in the bond layer can be received by integrating the stress field on the half-thickness cross-section of the bond (Eqs. (5a) ~ (5c)):

$$F^n = \int_{-wR}^{wR} \sigma_{zz} dx \tag{5a}$$

$$F^s = \int_{-wR}^{wR} \sigma_{xz} dx \tag{5b}$$

$$M = \int_{-wR}^{wR} x\sigma_{zz} dx \tag{5c}$$

As the relationship between force and displacement is determined, the bond model for a biconcave bond layer can be generated. The calculation of a biconcave bond model is based on the total displacement of a particle rather than on instantaneous increments; therefore, the previous deformation of the bond is not considered in the calculations and the reaction force depends on only current boundary conditions.

3. IMPROVEMENT OF CALCULATIONS

To implement the proposed model into DEM analysis, five issues of numerical analysis must be solved. (1) The DEM software PFC2D and the Dvorkin theory define shear displacement differently, and the conversion and updating of the correct shear displacement is complicated and inefficient. (2) The biconcave bond has a nonlinear moment-rotation relationship but no adequate equation can be used using the PFC2D. (3) PFC2D provides the relative rotational angle to obtain the moment, but the moment should be calculated based on the absolute rotational angle of each particle. (4) The original Dvorkin theory assumes that the bottom particle is immobile and that displacement occurs only in the upper particle, which causes difficulty when using the theory to analyze two mobile particles. (5) The stress field of the Dvorkin theory is asymmetrical in y axis on simple-loading situations (Fig. 4). To solve the abovementioned issues, motion decomposition and stress adjustment are used to modify the calculation process and increase accuracy.

3.1 Motion Decomposition for Shear Components

Although the Dvorkin theory can account for normal, shear, or rotational motion, adapting the shear displacement of PFC2D to the shear displacement of the Dvorkin theory is difficult. In Dvorkin theory, the input shear displacement must be the total displacement related to the initial state. In PFC2D, current shear displacement is not a tangential component but rather the contact displacement increment occurring over a time step (Itasca Consulting Group 2015). The local coordinate of the displacement increment changes with current contact vector, thus the total shear displacement is difficult to calculate using shear displacement increments. Therefore, the shear displacement increment provided by PFC2D cannot be adapted directly to biconcave bond model, and another means of determining total shear displacement is required.

Another issue is to acquire the nonlinear moment-rotation relationship for the numerical analysis. For existing linear bond models, forces are calculated in instantaneous increments, and new force increments are then added to the current force state. Researchers are not required to check the value of current stiffness because it is constant. However, the moment-rotation relationship of biconcave bond model is nonlinear, and the relationship between current angle and corresponding rotational stiffness is necessary during calculations.

Motion decomposition technique was used to solve this problem. When the shear displacement is applied on two particles, the particles would move to oppsite directions, which casues the shear deformation of bond (Fig. 5(a)). To consider this condition in numerical analysis, shear components are treated as the combination of normal and rotational motions, which has three components: one normal displacement W_{const} and two relatively rotational angle $\theta_{initial}^{[A]}$ and $\theta_{initial}^{[B]}$ (Fig. 5(b)). Hence, the determination of shear deformation can be easily obtained by calculating the normal displacement and rotations.

To adopt the biconcave bond model with motion decomposition technique, the total normal displacement W_{const} was recorded by accumulating instantaneous normal displacement ΔU^n:

$$W_{const} = \Delta U^n \Delta t \tag{6}$$

The particle's total rotational angle related to the center of the bond layer was obtained using the following procedure: at first, we define the x axis is the start of angle, and counterclockwise is positive. The unit vector of bond is $\vec{n}_i = (n_1, n_2)$, the upper particle is denoted as [A], and the bottom particle is denoted as [B]. The initial angle $\theta_{initial}^{[*]}$ (Fig. 6) during bond formation can be obtained from Eqs. (7a) and (7b) (Fig. 7(a)):

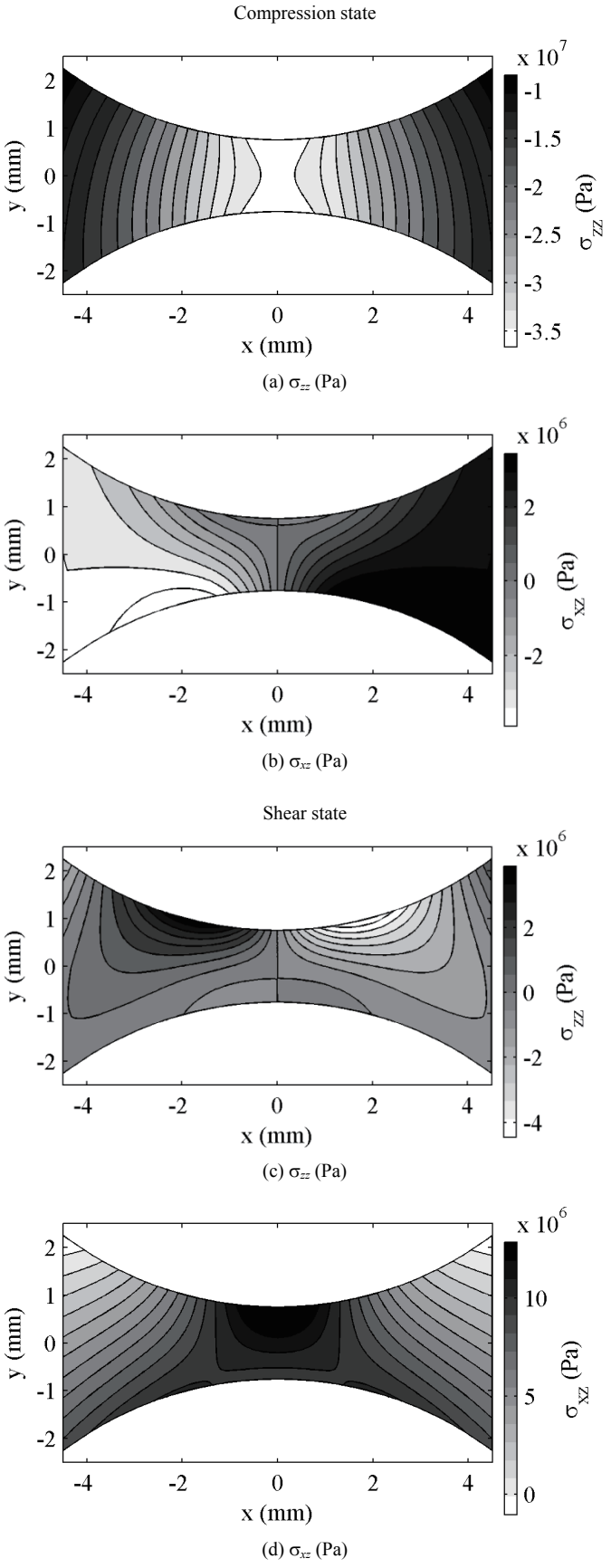

Fig. 4 Stress distribution in a simple loading case calculated according to the Dvorkin theory

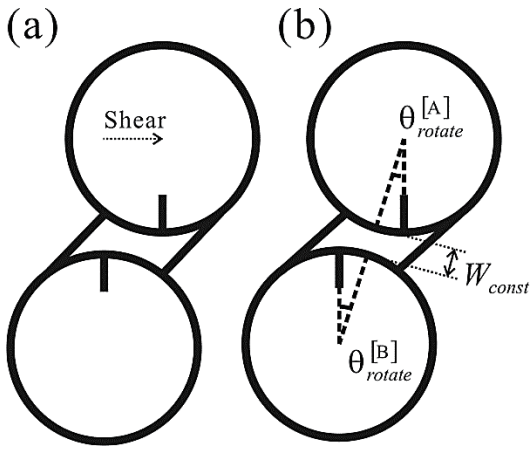

Fig. 5 Determination of particle movement. The shear displacement is transformed to a normal and rotational component to simplify the input parameters. (a) Deformation of the bond after particles move; (b) Scheme of numerical analysis

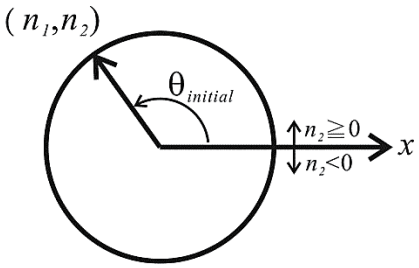

Fig. 6 The definition of initial angle $\theta_{initial}^{[*]}$

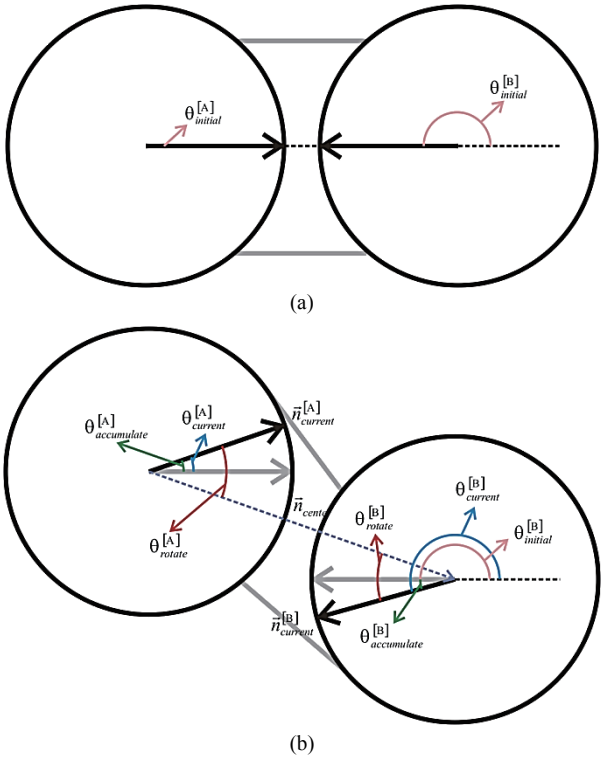

Fig. 7 The schematic diagram of each symbol in the process of motion decomposition (a) initial state when bond forming (b) current state when bond deforming

$$\theta_{initial}^{[A]}=\begin{cases}\cos^{-1}(n_1), & \text{if } n_2\geq 0.0\\ 2\pi-\cos^{-1}(n_1), & \text{if } n_2<0.0\end{cases} \tag{7a}$$

$$\theta_{initial}^{[B]}=\begin{cases}\cos^{-1}(-n_1), & \text{if } -n_2\geq 0.0\\ 2\pi-\cos^{-1}(-n_1), & \text{if } n_2<0.0\end{cases} \tag{7b}$$

$\theta_{initial}^{[A]}$ and $\theta_{initial}^{[B]}$ are the initial angle of particle [A] and [B] which is equal to the angle between $\vec{n}_i$ and x axis whose unit is radian. Then, the current vector of particle center to bond center can be tracked by accumulating the rotational angle of particle. The accumulated rotational angle can be obtained by:

$$\theta_{accumulate}^{[A]}=\omega_3^{[A]}\Delta t \tag{8a}$$

$$\theta_{accumulate}^{[B]}=\omega_3^{[B]}\Delta t \tag{8b}$$

$\omega_3^{[*]}$ is the angular velocity. The summation of initial angle of particle $\theta_{initial}^{[*]}$ and accumulated rotational angle $\theta_{accumulate}^{[*]}$ is the current angle of particle center to bond center $\theta_{current}^{[*]}$:

$$\theta_{current}^{[A]}=\theta_{initial}^{[A]}+\theta_{accumulate}^{[A]} \tag{9a}$$

$$\theta_{current}^{[B]}=\theta_{initial}^{[B]}+\theta_{accumulate}^{[B]} \tag{9b}$$

The vector of particle center to bond center $\vec{n}_{current}^{[*]}$ can be transformed by current angle $\theta_{current}^{[*]}$ through trigonometry:

$$\vec{n}_{current}^{[A]}=\left(\cos(\theta_{current}^{[A]}),\ \sin(\theta_{current}^{[A]})\right) \tag{10a}$$

$$\vec{n}_{current}^{[B]}=\left(\cos(\theta_{current}^{[B]}),\ \sin(\theta_{current}^{[B]})\right) \tag{10b}$$

The particle's total rotational angle related to the center of the bond layer $\theta_{rotate}^{[*]}$ can be obtained by the inner product of the vector of connection line $\vec{n}_{center}$ and the vector of particle center to bond center $\vec{n}_{current}^{[*]}$:

$$\theta_{rotate}^{[A]}=\begin{cases}\cos^{-1}(\vec{n}_{current}^{[A]}\cdot\vec{n}_{center}), \\ \quad \text{if } \cos^{-1}\left(\vec{n}_{current}^{[A]}\cdot(-n_2^{center},n_1^{center})\right)\leq\pi/2\\ -\cos^{-1}(\vec{n}_{current}^{[A]}\cdot\vec{n}_{center}), \\ \quad \text{if } \cos^{-1}\left(\vec{n}_{current}^{[A]}\cdot(-n_2^{center},n_1^{center})\right)>\pi/2\end{cases} \tag{11a}$$

$$\theta_{rotate}^{[B]}=\begin{cases}\cos^{-1}(\vec{n}_{current}^{[B]}\cdot-\vec{n}_{center}), \\ \quad \text{if } \cos^{-1}\left(\vec{n}_{current}^{[B]}\cdot(n_2^{center},-n_1^{center})\right)\leq\pi/2\\ -\cos^{-1}\left(\vec{n}_{current}^{[B]}\cdot-\vec{n}_{center}\right), \\ \quad \text{if } \cos^{-1}\left(\vec{n}_{current}^{[B]}\cdot(n_2^{center},-n_1^{center})\right)>\pi/2\end{cases} \tag{11b}$$

Figure 7(b) is the symbol meaning in the process of motion decomposition. Thus, the boundary conditions of the bond layer can be obtained easily at any time by tracking the current total displacement and then calculating its corresponding forces and moment, thereby solving Issue (2).

Motion decomposition also provides an absolute input rotational angle and solves Issue (3). In past simulations, relative rotational angles have been used to calculate moment, which is sufficient for beam theory. However, from a rigorous viewpoint, considering the rotational angle of both particles is more reasonable. For example, the reaction of one particle rotating 0.1 radians and another fixed particle differs from the reaction of one particle rotating 0.05 radians and another particle rotating –0.05 radians. For a relative rotational angle, the reactions are all the same, but in a motion decomposition framework, the reactions differ and each has distinct mechanical behavior.

3.2 Stress Adjustment for Relative Motion

The assumptions of the Dvorkin theory constrain the boundary condition of bonds, rendering the theory inappropriate for cases involving two mobile particles. Although relative displacement increments can be obtained through two mobile particles, updating relative displacement increments from two mobile particles to total displacement, which the Dvorkin theory requires, is prohibitively complex.

Stress adjustment is used to solve this problem by using the superposition of stress, which is a common technique in elastic analysis. The stress field of the bond layer is treated as the superposition of two occurrences: the upper particle moving independently of the lower particle and the lower particle moving independently of the upper particle (Fig. 8). After the movements are separated into two situations, the Dvorkin theory can be applied to obtain two temporary stress fields and superpose these fields to determine the current stress field:

$$\sigma_{xx}(x,z)=\sigma_{xx}^{[A]}(-x,-z)+\sigma_{xx}^{[B]}(x,z) \tag{12a}$$

$$\sigma_{xz}(x,z)=\sigma_{xz}^{[A]}(-x,-z)+\sigma_{xz}^{[B]}(x,z) \tag{12b}$$

$$\sigma_{zz}(x,z)=\sigma_{zz}^{[A]}(x,-z)+\sigma_{zz}^{[B]}(-x,z) \tag{12c}$$

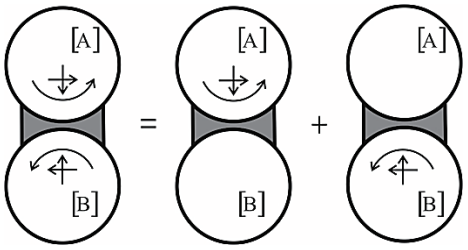

Fig. 8 The schematic diagram of stress adjustment. The movement of two particles has been separated as the superposition of two occurrences

The current stress field, comprising σ_{xx}, σ_{xz}, and σ_{zz}, is the combination of the two boundary conditions. The superscript denotes the stress field of two occurrences which particle is mobile. Through stress adjustment, the displacement of two mobile particles in numerical analysis can be considered by applying Dvorkin theory, and the stress field is symmetrical in simple-loading situations because of the superposition of similar loading conditions; thus, Issues (4) and (5) are solved.

4. CONTACT MODEL CONSTRUCTION

4.1 Process of Determining the Force-Displacement Relationship

To implement biconcave bond model in numerical simulations, a contact model must be established in the numerical software. The contact model in this study was developed using Microsoft Visual C++ 2005 and was based on the user-defined model (UDM) of PFC2D Version 4.0. Figure 9 is the flow chart of the biconcave bond model. To calculate the force-displacement relationship of biconcave bond model, the built-in variable (normal displacement W_{const}, shear displacement U_{const} and relative rotational angle θ) in the UDM of PFC2D are discarded. Instead, the normal displacement W_{const}, the particle's total rotational angle related to the center of the bond layer $\theta_{rotate}^{[A]}$ and $\theta_{rotate}^{[B]}$ are obtained by "motion decomposition" as the variable for calculating forces. After obtaining W_{const}, $\theta_{rotate}^{[A]}$, and $\theta_{rotate}^{[B]}$, the "stress adjustment" is adopted. The boundary conditions of the bond are separated into normal displacement for W_{const} / 2 and anglefor $\theta_{rotate}^{[A]}$. Another boundary condition is normal displacement for $W_{const}/2$ and rotational angle for $\theta_{rotate}^{[B]}$. A follow-up procedure is calculated by applying the Dvorkin theory, and then superposition to determine the adjusted stress field by Eqs. 10(a) ~ 10(c). Finally the corresponding forces are easily obtained by Eqs. 5(a) ~ 5(c).

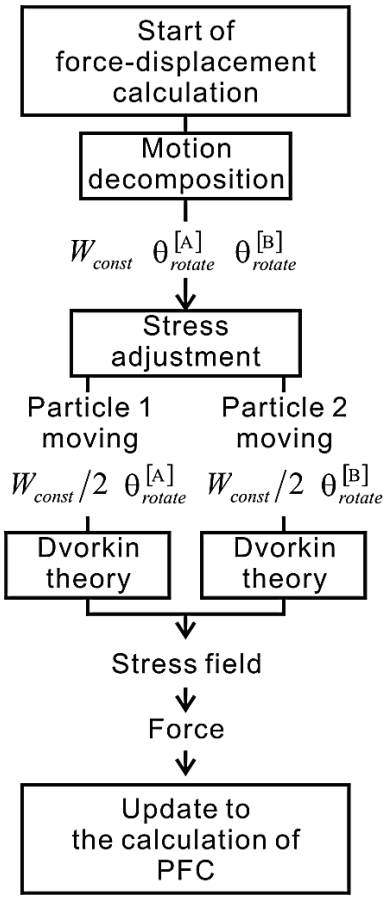

Fig. 9 Process of determining the force-displacement relationship in a biconcave bond model

4.2 Failure Criterion

The failure criterion of the biconcave bond model is based on maximum shear and tension stress on the center cross-section of the bond. The failure of bond is determine by maximum stress. Equation (13) shows the failure criteria:

$$\begin{cases} \left|\sigma_{xz}\left(x, h(x)/2\right)\right| \geq S_s\ ,\ -wR \leq x \leq wR\ , \text{ shear failure} \\ \sigma_{zz}\left(x, h(x)/2\right) \geq S_n\ ,\ -wR \leq x \leq wR\ , \text{ tension failure} \end{cases} \tag{13}$$

where S_s is the shear strength and S_n is the tensile strength.

4.3 Operation in Numerical Analysis

To confirm the biconcave bond model operate in PFC2D accurately, a comparison between theoretical analysis which is calculated by MATLAB and simulation results which obtained by PFC2D has been adopted. A simple test was performed using unitary movement (compression, shear for 1.7×10^{-4} m and rotation for 1.7×10^{-3} radian) for two equal-sized particles (Fig. 10) to ensure that the model functioned as intended. The radii of both particles were 7.5×10^{-3} m. Six required parameters, elastic moduli, were set as 4.4×10^{9} Pa, and the Poisson's ratio was 0.27. The bond thickness factor t was set at 0.2, the bond radius factor w was set at 0.6, the mean bond thickness was 1.5×10^{-3} m, and the radius of layers was 9.0×10^{-3} m. The strength of bond S_s and S_n was set to infinity to prevent bond breakage. The results indicated that the force-displacement relationship determined by PFC2D supported our hypothesis. Only the shear direction situation exhibited a small error in normal force calculation. In addition, the required parameters for the biconcave bond model, elastic moduli, Poisson ratio, normal and shear strength, can be obtained by uniaxial compression test and direct shear test which the specimen is cement material. The bond thickness factor t and the bond radius factor w are choose by users, and it is possibly correlated with the porosity or grain-cement content ratio.

5. CHARACTERISTICS OF A SINGLE BOND

To investigate the accuracy of biconcave bond model, the stress fields of biconcave bond model and numerical elastic solution are compared at first. And then we investigate the influence between bond geometry and stiffness to investigate the force-displacement relationship. Finally, a nonlinear force-displacement relationship is established based on the proposed model, in which the parallel bond model do not appear this special characteristic.

5.1 Stress Distribution

To confirm the accuracy of the biconcave bond model, a comparison of stress field with analytical elastic analysis is required. However, until now no analytical elastic solution has been proposed, therefore, the FEM numerical elastic analysis is treated as the approximate solution of exact elastic solution. Although the calculations of bond forces depends solely on the cross-sectional stress profile, this study still compare the entire stress field of the biconcave bond to ensure that the simulation results are precise. The FEM analysis is performed using software ABAQUS, and the stress field of the biconcave bond model in this section is calculated in MATLAB because of the calculation results of PFC2D do not provide stress field in a single bond. The object of analysis is a biconcave elastic block and the shape is shown as Fig. 3. The boundary condition of FEM simulation and biconcave bond model calculated in MATLAB are the same, the upper and bottom boundary, which is treated as the particle-cement interface, is set as displacement control boundary, and the displacements are assumed to be the particle's normal, shear, and rotational movements. The other boundaries are traction-free with stress set to zero.

The boundary condition of the bond layer shown in Figs. 11 and 12 is under compression and shear loading. The radii of both particles are 7.5×10^{-3} m, and the geometric factors t and w are 0.2 and 0.6, respectively, which indicates that bond thickness is 1.5×10^{-3} m and that the radius of the layer is 4.5×10^{-3} m. The lower particle is fixed and the upper particle exhibits 10^{-5} m of normal and shear displacement.

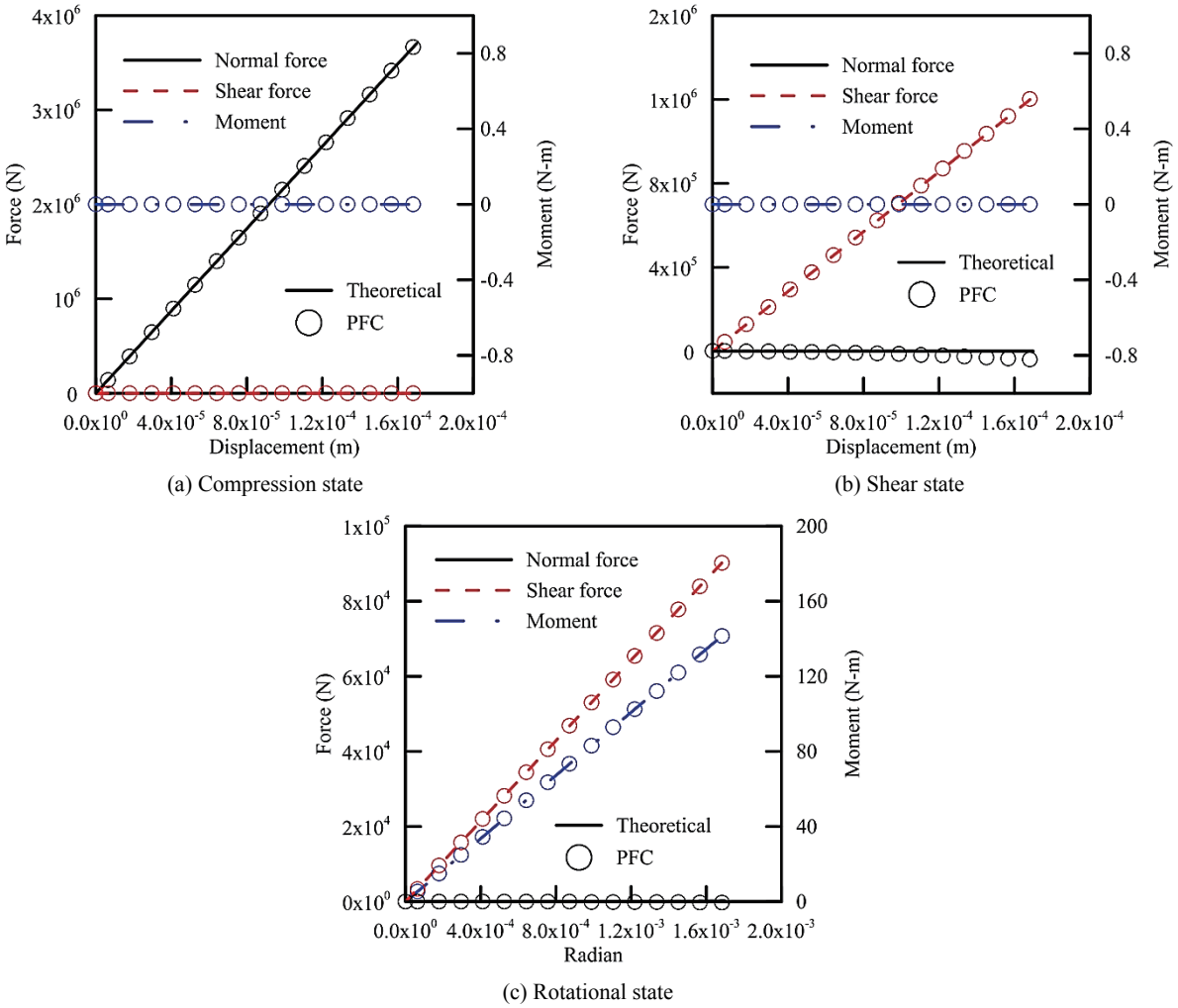

(a) Compression state

(b) Shear state

(c) Rotational state

Fig. 10 Operations of biconcave bond (line) in PFC^{2D} (circle) under (a) compression, (b) shear, and (c) rotational states

Figure 11 displays three stress fields in the FEM elastic analysis and in the biconcave bond. The major information required to calculate forces, σ_{xz} and σ_{zz} is provided in two simple motions. Compared with Fig. 4, the trend of stress distribution in biconcave bond model is more closer to numerical elastic analysis. The asymmetry problem is solved using stress adjustment in the biconcave bond model. For the stress profile on center cross-section of the bond layer (Fig. 12), the results obtained by Dvorkin theory has a redundant stress distribution (Figs. 12(b) and 12(c)), which introduces errors into the calculations of forces. The redundant stress is ascribed to imperfect elastic solution of Dvorkin theory, and the biconcave bond model also ameliorates this problem by using stress adjustment. Figures 12(b) and 12(c) demonstrate that the stress profiles obtained by biconcave bond model nearly fit the FEM analysis results.

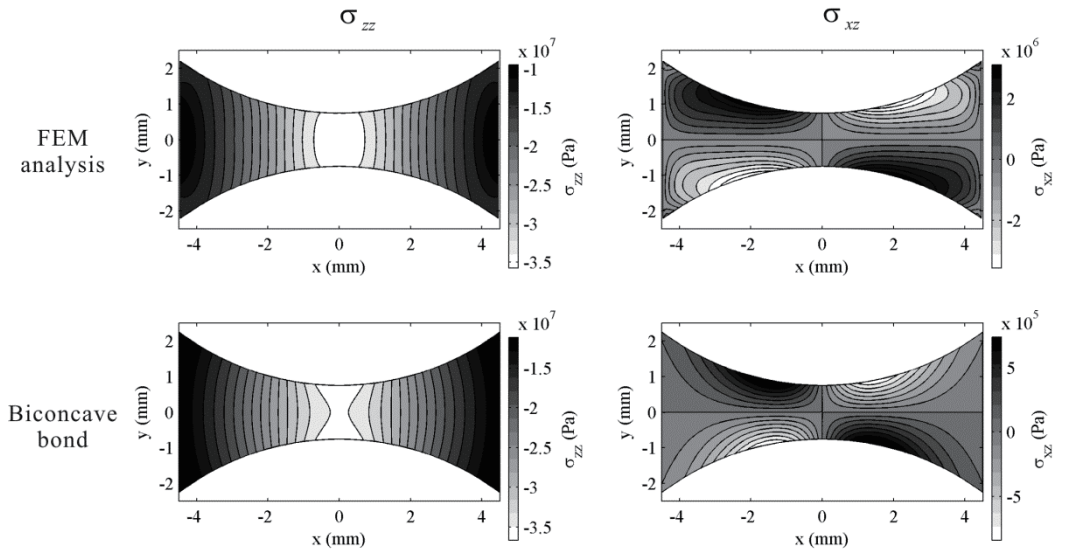

(a) Compression state

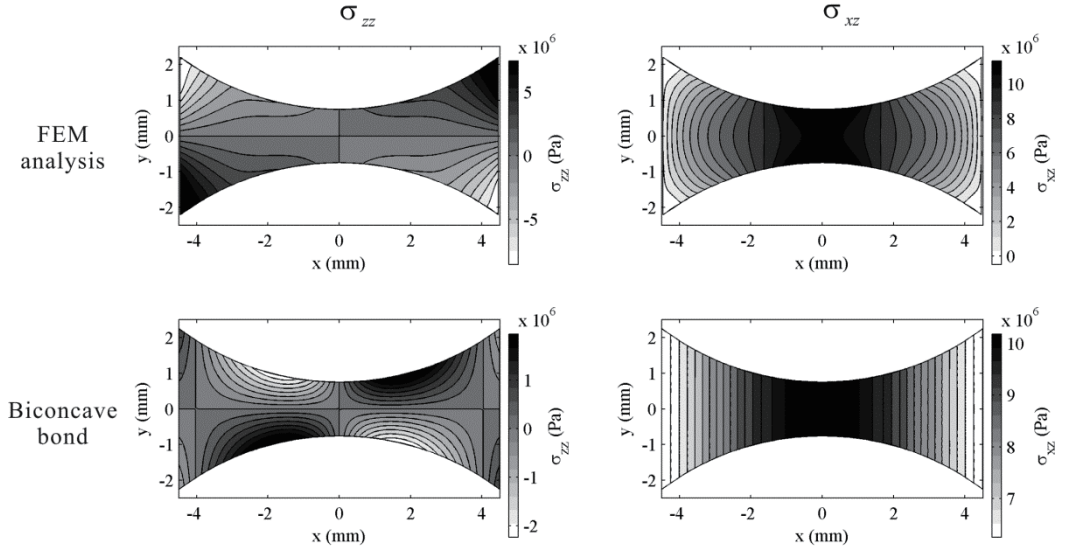

(b) Shear state

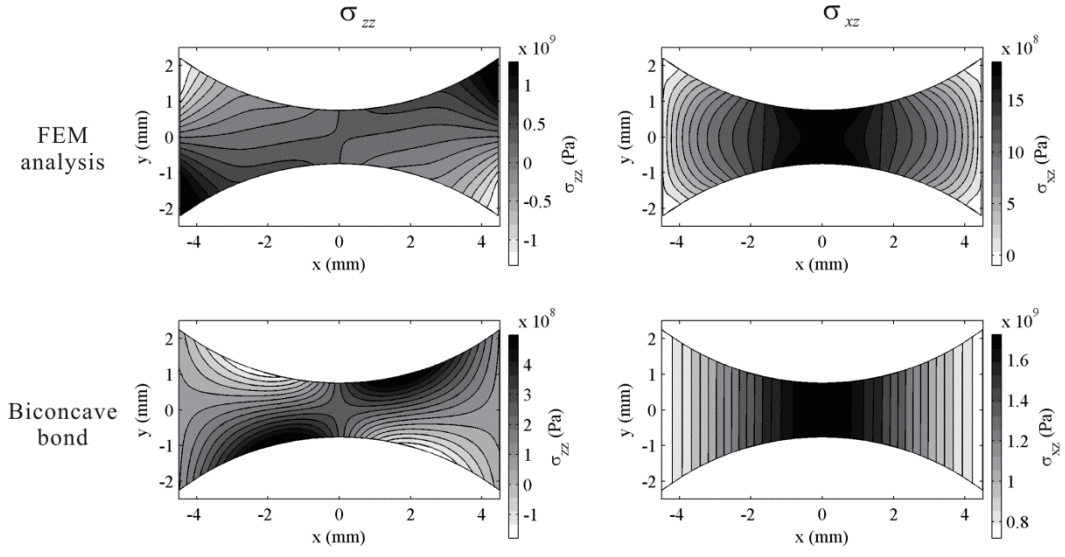

(c) Rotational state

Fig. 11 Comparison of stress distribution between the FEM result and the proposed model

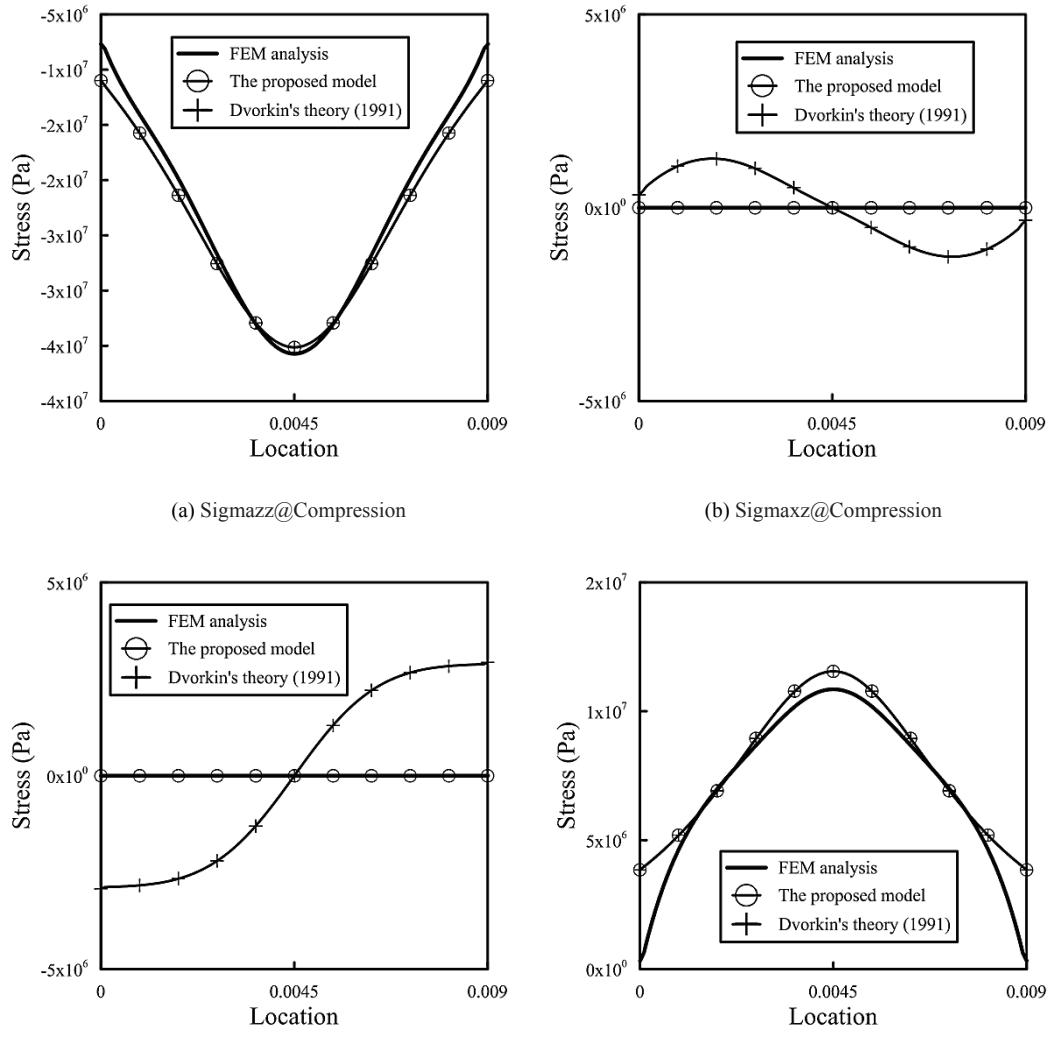

(a) Sigmazz@Compression

(b) Sigmaxz@Compression

(c) Sigmazz@Shear

(d) Sigmaxz@Shear

Fig. 12 Stress distribution along the cross-section after the stress adjustment

5.2 Relationship of Stiffness and Geometry

To explore the geometric effect of the bond layer, a series of shapes with different size are simulated. The geometric factors t and w are assigned values from 0.1 to 0.99, woven into 9801 types of bond layers. Figure 13 shows the variations of stiffness under normal compression mode, shear mode and rotational mode, respectively. Figures 13(a) and 13(b) illustrate that the relationship between stiffness and geometry is similar on compression and shear mode, with the exception of the stiffness value. Figure 13(c) exhibits the most notable variation of the three figures: at an increased thickness, the effect of the radius is more substantial in Fig. 13(c) than in the other two figures. All three figures demonstrate that the stiffness of the bond layers has a nonlinear tendency to increase as bond radius increases and to decrease as bond thickness increases (Fig. 14(a)). In parallel bond model, the relationship between stiffness and shape is linear. The shape is treated as a square bond, and only the radius of the bond shape can be altered. Even normal, shear, and rotational force-displacement relationship of a biconcave shape bond can be reproduced by parallel bond model with back analysis individually, matching all three simultaneously is difficult because of the theoritical restrictions of parallel bond model, which use normal stiffness to control normal and rotational motion simultaneously and cause normal stiffness hard to be calibrated with a suitable value.

5.3 Nonlinearity of Rotational Stiffness

In biconcave bond model, the stiffness varies with the material properties, geometry, and current boundary conditions. Therefore, the stiffness of biconcave bond model is not a fixed value. Figure 15 illustrates three comparisons of stiffness between biconcave bond model and parallel bond model. The displacement in normal and shear direction is 10^{-5} m, the rotational angle is 1 radian, and the geometry of the biconcave bond is t = 0.4 and w = 0.6. Figures 15(a) and 15(b) demonstrate that stiffness is constant in both normal and shear directions, and that the stiffness of biconcave bond model is higher than that of parallel bond model, which agree with the data in Figs. 13(a) and 13(b). In Fig. 15(c), the rotational stiffness of biconcave bond model is nonlinear and the increase rate decreases as the radial value increases. Furthermore, FEM analysis also demonstrates this phenomenon, and parallel bond model do not exhibit such behavior. The nonlinearity of rotational stiffness is originated from the shape of bond. In this study, the moment is obtained

from Eq. (5c). The neutral axis is located at $x = 0$, which is at the center of bond. At the start of particle rotation, one side of the normal stress is tensile, and the other side is compression; however, when the rotational angle increases, the neutral axis will move to compression zone which induces more tensile stress and less moment. Hence, the rotational stiffness exhibts nonlinear, and the increase rate of moment will decrease when rotational angle gradually arise. The results confirm that biconcave bond model is more appropriate for describing the mechanical behavior of biconcave shape bond layers than parallel bond model.

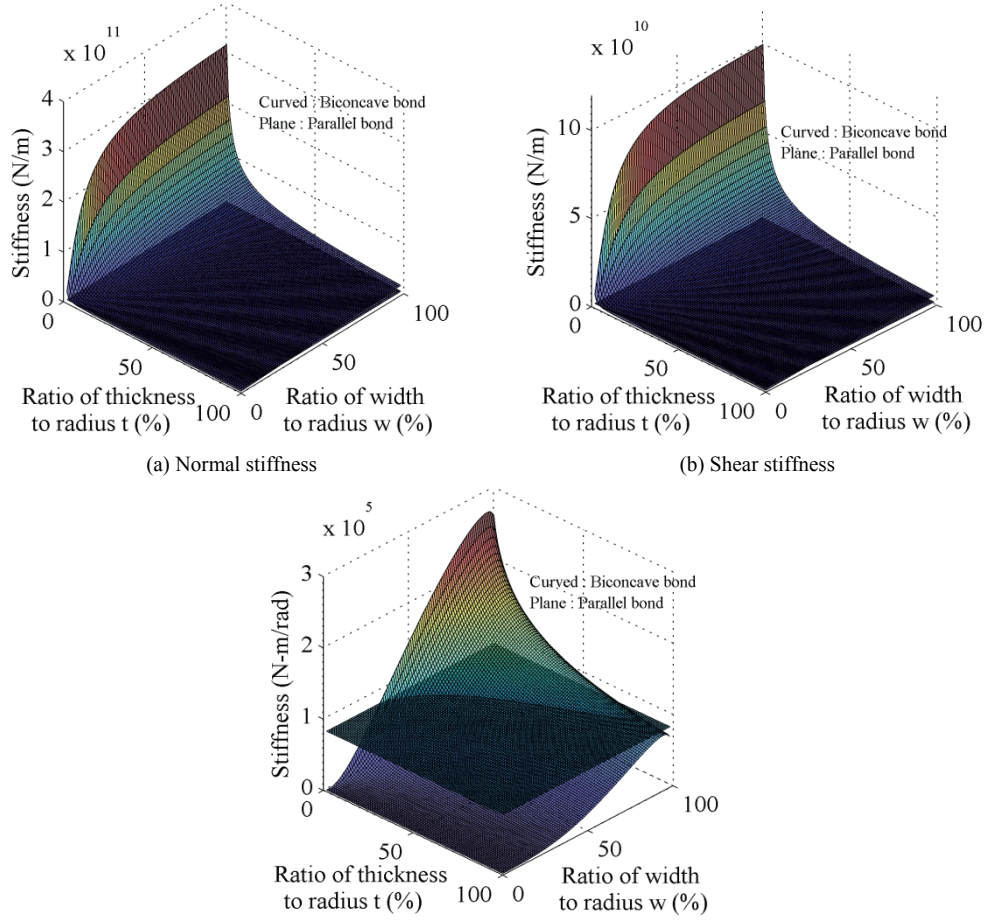

Fig. 13 Influence of bond geometry on the biconcave bond and parallel bond models

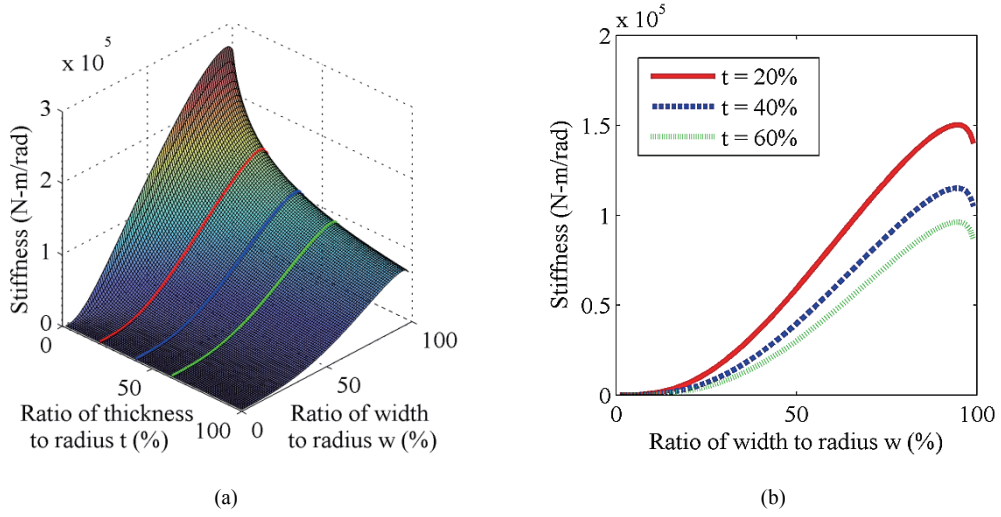

Fig. 14 The rotational stiffness of the biconcave bond tends to decay when thickness increases

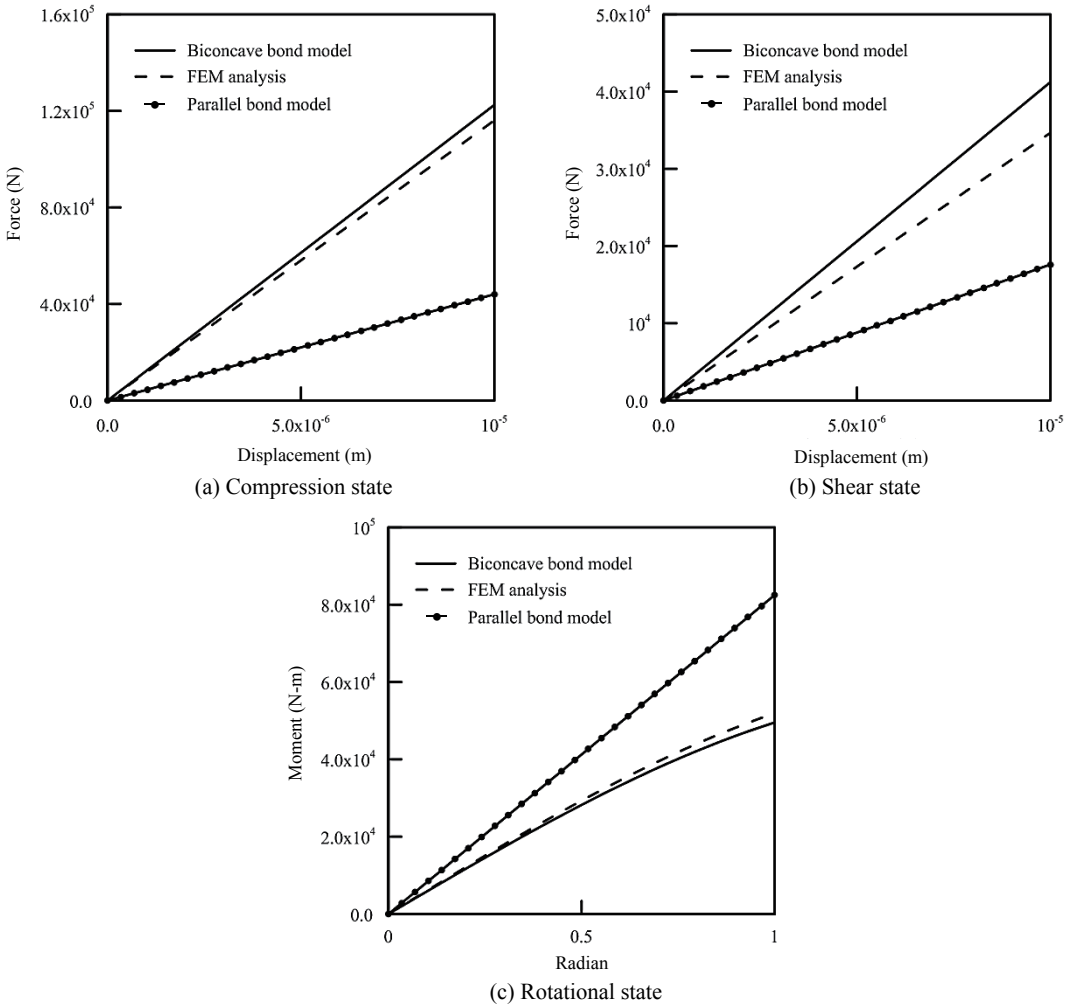

(a) Compression state (b) Shear state

(c) Rotational state

Fig. 15 Force-displacement relationship in (a) compression, (b) shear, and (c) rotational states

6. VERIFICATION OF CONTACT MODEL

To assess the validity of the proposed model on cemented granular material, an assembly of equal-sized circular aluminum rods was cemented as the specimen for the biaxial compressive test. Two types of rods were adopted. The first type was 6 mm in diameter and 60 mm in length, and the second type was 10 mm in diameter and 60 mm in length. The first type of specimen contained 15 layers of 6 mm rods, with each layer including six or seven rods (Fig. 16). The rods were arranged in dense packing with a porosity of 9.32%. To reflect the characteristics of cementation, resin (polyvinyl acetate) was used to glue the rods, and the shape of cementation formed biconcave shape between two rods. To facilitate the experimental observations, black paint was sprayed on the surface of the specimen. Figure 16(b) illustrates a DEM model for simulation of biaxial compressive tests. The upper and lower boundaries were set rigid. The lateral boundary was flexible and allowed to deform. During loading, the upper wall was moved downward at a constant velocity the same as the actual test. For the second type of specimen, it was composed of 9 layers of 10 mm rods, with each layer including three or four rods (Fig. 17). The corresponding numerical model is shown in Fig. 17(b). In order to investigate the influence of confining pressure on the cemented rod assembly, three levels of confining pressure were applied: 0, 51, and 71 kPa. Following this, the specimens under different confining pressure were sheared at a rate of 0.05 mm/sec.

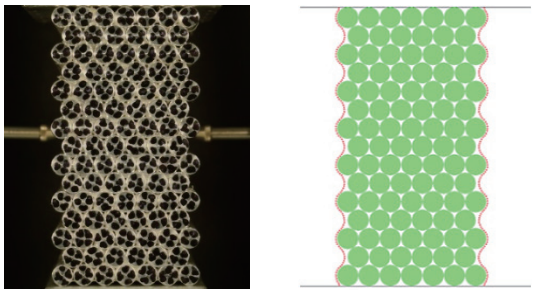

(a) (b)

Fig. 16 Cemented rod specimen of biaxial compressive test with 6 mm rod specimen and the corresponding DEM model

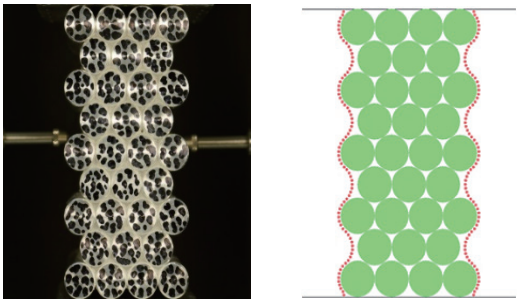

(a) (b)

Fig. 17 Cemented rod specimen of biaxial compressive test with 10 mm rod specimen and the corresponding DEM model

For the properties of aluminum and resin, the material density ρ of aluminum is 2702 kg/m^3; the Young's modulus is 70 GPa; the Poisson's ratio is 0.33; the inter-rod friction angle is 20.9°. For the resin (polyvinyl acetate), the solidified strength in dry condition is 0.79 MPa. The required numerical parameters were listed in Table 1. Remarkably, slightly different bond strength is applied in two cases because the resin was casted well in 10 mm rods case but few flaws existed in 6 mm rods case. Therefore, the strength of 10 mm case is close to solidified strength of resin and the strength of 6 mm case is reduced.

Figure 18 shows the stress-strain curves obtained by experiment and numerical simulation. It can be seen the simulated and experimental curves under different confining pressures shown in Fig. 19 were fairly consistent and the values of peak strength were also similar. Both the simulated and actual behaviors of the cemented rod assembly revealed that shear displacements increased linearly at the early loading stage, and the stiffness increased with increasing application of normal pressure. When the shear stress approached the failure state, strain-softening behavior was observed and stress dropped gradually after the peak. The discrepancy of post-peak stress-strain curve between experiment results and simulation results is originate from the difference of post-peak material behavior. In experiment, the cement material is resin, which is easily to deform and extremely ductile. However, in simulation, the biconcave bond model only exists at the pre-break stage, when forces exceed bond strength, it will break, and the mechanical behavior will switch to linear contact model which is unable to describe ductile behavior. Furthermore, Fig. 19 compares the failure patterns of the experiments with the DEM analyses for the two types of speimen, respectively. It can be seen that the patterns from the analyses are similar to those from the experiments.

Based on above simulation results, the biconcave bond model is capable of predicting the mechanical behavior of cemented granular material. Compared with exising bond models, the parameters of the proposed model are easily determined from the properties of cementation. It provides a feasible way to investigate the relationships between microproperties and macromechanical behaviors. Last but not least, the limitation of using the proposed model is notified that the calculation is time consuming and the post peak behavior cannot be well predicted.

Table 1 Parameters of simulations

Rods		Resin	
Density	2702 kg/m^3	E	45 MPa
Rod length	0.06 m	v	0.3 mm
Friction angle	20.9°	Thickness	0.2 mm
Normal stiffness	23.2 MPa	Width	0.6 mm
Shear stiffness	1.987 MPa	Normal strength	
		(For D = 6 mm)	0.4 MPa
		(For D = 10 mm)	0.63 MPa
		Shear strength	
		(For D = 6 mm)	0.67 MPa
		(For D = 10 mm)	1.04 MPa
Lateral boundary			
Normal stiffness	12 MPa	Shear stiffness	4.8 MPa
Normal bond stiffness	0.2 MPa	Shear bond stiffness	0.02 MPa
Normal bond strength	10^{93} MPa	Shear bond strength	10^{93} MPa

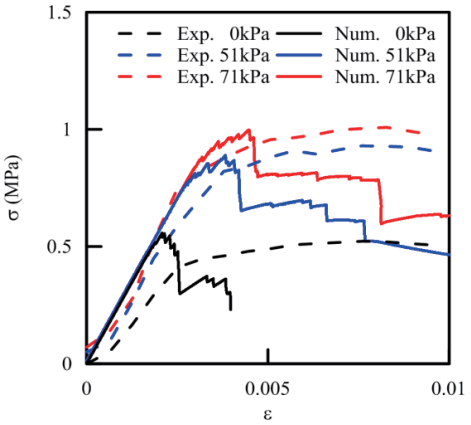

(a) 6 mm rod specimen

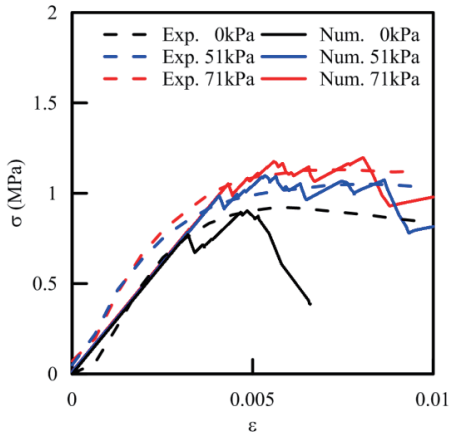

(b) 10 mm rod specimen

Fig. 18 Comparison of stress-strain curves between experiments and simulations

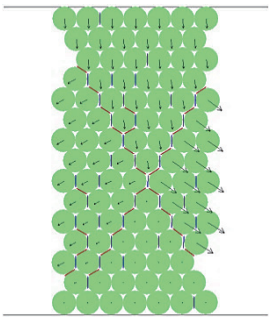

(a) Simulation of 6 mm rod

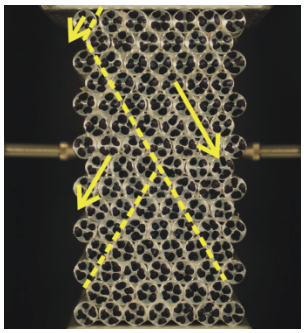

(b) Experiment of 6 mm rod

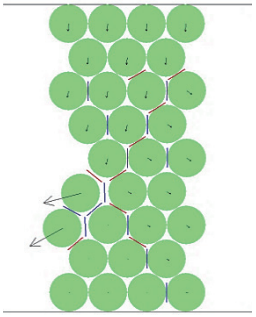

(c) Simulation of 10 mm rod

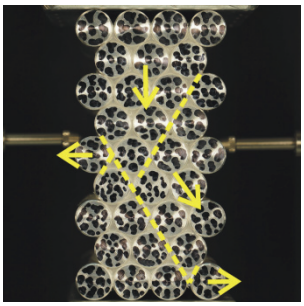

(d) Experiment of 10 mm rod

Fig. 19 Failure patterns of experiments and simulations

7. CONCLUSION

This study proposed a biconcave shaped bond model for DEM analysis that can be used to consider the realistic shape of a bond layer. To simulate the model with the DEM, a modified superposition method that improved the accuracy and symmetry of the stress field was developed. The method of motion decomposition altered the input parameters, allowing the biconcave bond to function in PFC2D and providing meaningful input parameters by considering both particle rotation and relative motion. The simulated stress contours indicated that the results of the biconcave bond model were correlated closely with the results of the FEM analysis. The shape of the bond layer influenced its stiffness substantially. As the thickness of the layer increased, stiffness decreased, and the variation of the radius exhibited conflicting results. Biconcave bond model displayed nonlinear rotational stiffness in biconcave bond layers. The results are consistent with that of the FEM analysis. Finally, biconcave bond model was successfully implemented into DEM software PFC2D. The proposed model was further verified with the behavior of cemented assemblies of aluminum rod. This innovative bond model can help researchers further understand the micro- macro relationship of cemented granular materials which the geometry of bond is similar to biconcave shape.

ACKNOWLEDGEMENTS

The authors acknowledge the contribution of Mr. Yu-Gang Hu and Szu-Wei Lee in completion of the work. The authors also thank the Ministry of Science and technique, Taiwan, for financially supporting this research under Contract 103-2221-E-002-163 and 104-2221-E-002-162.

REFERENCES

Brown, N.J., Chen, J.F., and Ooi, J.Y. (2014). "A bond model for DEM simulation of cementitious materials and deformable structures." *Granular Matter*, **16**(3), 299–311.

Chang, Y.L., Chen, T.H., and Weng, M.C. (2012). "Modeling particle rolling behavior by the modified eccentric circle model of DEM." *Rock Mechanics and Rock Engineering*, **45**(5), 851–862.

Chiu, C.C., Wang, T.T., Weng, M.C., and Huang, T.H. (2013). "Modeling the anisotropic behavior of jointed rock mass using a modified smooth-joint model." *International Journal of Rock Mechanics and Mining Sciences*, **62**, 14–22.

Delenne, J.-Y., El Youssoufi, M.S., Cherblanc, F., and Bènet, J.-C. (2004). "Mechanical behaviour and failure of cohesive granular materials." *International Journal for Numerical and Analytical Methods in Geomechanics*, **28**(15), 1577–1594.

Ding, X.B. and Zhang, L.Y. (2014). "A new contact model to improve the simulated ratio of unconfined compressive strength to tensile strength in bonded particle models." *International Journal of Rock Mechanics and Mining Sciences*, **69**, 111–119.

Duan, K., Kwok, C.Y., and Tham, L.G. (2015). "Micromechanical analysis of the failure process of brittle rock." *International Journal for Numerical and Analytical Methods in Geomechanics*, **39**(6), 618–634.

Dvorkin, J., Mavko, G., and Nur, A. (1991). "The effect of cementation on the elastic properties of granular material." *Mechanics of Materials*, **12**, 207–217.

Dvorkin, J. and Yin, H.Z. (1995). "Contact laws for cemented grains-implications for grain and cement failure." *International Journal of Solids and Structures*, **32**(17-18), 2497–2510.

Hertz, H. (1882). "Ueber die berührung fester elastischer körper." *Journal Für Die Reine Und Angewandte*, **1882**(92), 156–171.

Itasca Consulting Group (2015). *PFC2D (Particle Flow Code in 2 Dimensions)*, Version 4.0, Minneapolis, MN, ICG.

Jiang, M.J. and Zhu, H.H. (2007). "An interpretation of the internal length in Chang's couple-stress continuum for bonded granulates." *Granular Matter*, **9**(6), 431–437.

Kozicki, J. and Donzé, F.V. (2008). "A new open-source software developed for numerical simulations using discrete modeling methods." *Computer Methods in Applied Mechanics and Engineering*, **197**(49-50), 4429–4443.

Mas Ivars, D., Pierce, M.E., Darcel, C., Reyes-Montes, J., Potyondy, D.O., Paul Young, R., and Cundall, P.A. (2011). "The synthetic rock mass approach for jointed rock mass modelling." *International Journal of Rock Mechanics and Mining Sciences*, **48**(2), 219–244.

Ng, T. (2006). "Input parameters of discrete element methods." *Journal of Engineering Mechanics*, **132**(7), 723–729.

Obermayr, M., Dressler, K., Vrettos, C., and Eberhard, P. (2013). "A bonded-particle model for cemented sand." *Computers and Geotechnics*, **49**, 299–313.

Pilkavičius, S., Kačianauskas, R., and Norkus, A. (2013). "Investigation of normal contact interaction between two bonded spherical particles with interface layer." *Mechanika*, **18**(6), 632–639.

Potyondy, D.O. and Cundall, P.A. (2004). "A bonded-particle model for rock." *International Journal of Rock Mechanics and Mining Sciences*, **41**(8), 1329–1364.

Potyondy, D.O. (2011). "Parallel-bond refinements to match macro properties of hard rock." *Proceedings of the Second International FLAC/DEM Symposium*, Melbourne, Australia, Itasca, 459–465.

Walton, O.R. and Braun, R.L. (1986). "Viscosity, granular-temperature, and stress calculations for shearing assemblies of inelastic, frictional disks." *Journal of Rheology*, **30**(5), 949–980.

Wang, Y.H., Lau, Y.M., and Gao, Y. (2014). "Examining the mechanisms of sand creep using DEM simulations." *Granular Matter*, **16**(5), 733–750.

Weng, M.C. and Li, H.H. (2012). "Relationship between the de-formation characteristics and microscopic properties of sandstone explored by the bonded-particle model." *International Journal of Rock Mechanics and Mining Sciences*, **56**, 34–43.

Zhu, H., Chang, C.S., and Rish, III, J.W. (1996). "Normal and tangential compliance for conforming binder contact I: Elastic binder." *International Journal of Solids Strucrures*, **33**(29), 4337–4349.